

# Stochastic optimization of high-altitude airship envelopes based on Kriging method

Adrián García-Gutiérrez<sup>a</sup>, Jesús Gonzalo<sup>a</sup>, Diego Domínguez<sup>a</sup>, Deibi López<sup>a</sup>

<sup>a</sup>Universidad de León, Aerospace Engineering Area, Campus de Vegazana S/n, León, 24071, Spain

---

## Abstract

High-altitude airships can be used to transport substantial payloads to the stratosphere and remain there over long periods of time. In this paper, an algorithm for the design of high-altitude airship envelopes, accounting for uncertainties, is developed and applied. The algorithm is based on the non-intrusive polynomial chaos expansion scheme, which is employed to build a stochastic kriging metamodel. Two uncertainties are examined and characterized: 1) the stratospheric wind fluctuations using reanalysis datasets and 2) the variability in the turbulence levels. The method results are discussed to address the relevancy of the uncertainties. It is found that the drag coefficient of stratospheric envelopes can vary by as much as 30 percent. As a case of study, an ideal stratospheric airship is considered, operating at an altitude of 20 km, at a latitude of 30°N and carrying a payload of 250 kg. The baseline design follows the shape of the ZHIYUAN-1 envelope and the cost function to be minimized is the average mission drag coefficient. Due to the new method, a significant reduction (4%) of the average drag of the aircraft is achieved.

*Keywords:* airship, drag reduction, robust design, stochastic optimization

---

## Nomenclature

$Au_i$	Parameters of the CST parameterization
$C_{D,v}$	Volumetric drag coefficient
$C_{D,p}$	Volumetric pressure drag coefficient

$C_{D,v}$	Volumetric friction drag coefficient
$\mathcal{C}_D$	Stochastic operator used to compute the $C_{D,v}$
$\hat{\mathcal{C}}_D$	Approximation of the function $\mathcal{C}_D$
$C_{N_2}^{N_1}$	Class function
CFD	Computational fluid dynamics
CDF	Cumulative distribution function
E	Expectation operator
$F$	Cost function
FFD	Free-form deformation
HAPS	High-Altitude Pseudo-Satellites
$k$	Turbulence kinetic energy
$K_v$	Speed constant
$L$	Airship length
Ma	Mach number
MC	Monte Carlo method
$MSE$	Mean squared error
NIPC	Non-intrusive polynomial chaos
PDF	Probability density function
RBF	Radial basis function
Re	Reynolds number
RMS	Root mean square
$\mathbf{X}$	Multivariate random variable
$S_i$	Univariate random variable/ Component shape function
SL	Sea level
$S_u$	Shape function equation for the upper surface
$Tu_\infty$	Turbulence levels (%)
$U$	Wind velocity
UQ	Uncertainty Quantification
$V$	Airship volume
$\mathbf{Y}$	Multivariate stochastic function

$\hat{Y}_i$	NIPC expansion coefficients
$\bar{w}$	Velocity
$\alpha$	Angle of attack
$\Delta\zeta_{hull}$	Thickness of the trailing edge
$\phi$	One dimensional polynomial basis function
$\Phi_i$	Multivariate orthogonal polynomial basis function
$\psi$	Dimensionless coordinate $x/c$
$\zeta$	Dimensionless coordinate $y/c$
$\mu$	Kinematic viscosity/mean
$\rho$	Air density
$\nu$	Kinematic viscosity
$\nu_t$	Turbulence viscosity
$\omega$	Turbulence specific dissipation rate
$\sigma$	Standard deviation

## 1. Introduction

In recent years, there is a growing interest in High Altitude Pseudo-Satellites (HAPS) due to their relevant applications in Telecommunications, Earth Observations and Defense [1]. Although the technical difficulties are still very defiant, recent advances in the field of solar cells, batteries or fabric materials have overcome traditional limitations and notably improved the feasibility of those platforms.

Energy management onboard the platform is a key issue that limits platform size and flight endurance. Related to this, the drag coefficient of the airship plays a very relevant role, as most of the energy consumption required to keep the platform flying is used to compensate aerodynamic drag. At the end, that means drag value strongly conditions the required size of the batteries, the solar panels and even the propellers [2]. About the 60-70% of the total drag is due to the hull [3]. Thus, to reduce the total drag, the first step is to improve the

15 aerodynamic design of the hull.

16 Previous studies have explored the shape optimization of stratospheric air-  
17 ship [3, 4] and, also, have studied their aerodynamic characteristics [5][6][7] and  
18 the effect of the propeller [4].

19 However, this studies suffer from the fact that they do not address the ro-  
20 bustness of the designs. Therefore, a poor performance might be obtained under  
21 off-design operational conditions attending to mission phases, maneuvers or en-  
22 vironmental conditions.

23 Typically, the robustness of designs has been analyzed in multidisciplinary  
24 studies [8, 9] integrating different disciplines such as energy management, ther-  
25 mal control, structural and aerodynamic design [10, 11].

26 This study, however, focuses on the way in which the robust aerodynamic  
27 design of stratospheric airship hulls can improve the overall performance of the  
28 mission. Although a full discussion of all the uncertainties in the hull design is  
29 beyond the scope of this study, two of the most relevant environmental effects  
30 impacting aerodynamics are considered: the variation of the wind intensity and  
31 air turbulence levels.

32 Despite many designers consider constant wind (for a fixed altitude) in their  
33 analysis, the wind intensity is better fit by a Weibull distribution [12]. The  
34 impact of this variation in the mean drag coefficient of the hull has received  
35 scant attention in the research literature. Furthermore, due to the low density,  
36 the Reynolds number of these airships is lower than in the traditional ones.  
37 Thus, aerodynamic coefficients can be significantly affected by wind turbulence  
38 levels in the far-field region [13].

39 Generally speaking, the introduction of uncertainties into the design has  
40 been done following different approaches. For example, Kumar [14] combined  
41 the non-intrusive polynomial chaos (NIPC) with adjoint formulations using the  
42 CFD code SU2 [15]. The method was applied to a 2D transonic airfoil under  
43 uncertainties in the Mach number and angle of attack. However, these uncer-  
44 tainties were not related to real operational conditions. The study was focused  
45 on the design method and, thus, the uncertainty modeling was not studied in

46 depth. The main disadvantage of this method is that the adjoint formulation  
47 can be difficult to implement in some cases —the adjoint system equations are  
48 not the same as the equations of the system that is being modeled, so the solvers  
49 have to be customized—.

50 As alternative, Liatsikouras *et al.* [16] proposed a new method based on  
51 evolutionary algorithms combined with the non-intrusive Polynomial Chaos.  
52 They applied it to the optimization of 2D airfoils and S-Bend Duct. This method  
53 can be easily adapted to a broad range of situations, however, it is based on  
54 an on-line trained metamodel implemented within an evolutionary algorithm.  
55 This might be a problem if the computational load is high enough to require  
56 High Performance Computing centers. In that case, an off-line approach is more  
57 adequate.

58 Within the naval field, Serani *et al.* [17] proposed a new algorithm for ship  
59 hull optimization based on 4 steps 1) dimensionality reduction of the design  
60 space, 2) adaptive metamodeling, 3) uncertainty quantification and 4) multi-  
61 objective global optimization algorithms. Its final design achieved an expected  
62 mean value of total drag of -2.8 %.

63 Following previous studies on robust optimization, the design algorithm con-  
64 sists of three main parts:

- 65 1. First, we determine the performance of a particular design taking into ac-  
66 count the different uncertainties following one of the available Uncertainty  
67 Quantification (UQ) techniques. The NIPC seems to be the best option  
68 based on its fast convergence and its easy implementation.
- 69 2. Second, a metamodel is built using results from CFD simulations. That  
70 metamodel will be used to easily compute the mean drag coefficient of the  
71 airship as a function of some design variables. There are several kinds of  
72 metamodels (also known as surrogate models), but kriging metamodels  
73 provide a good balance between computational resources and accuracy  
74 [18][19]. Although RBF (Radial basis function) networks have not been  
75 used in this work, they can be a good alternative, as shown in several

76 studies [20].

77 3. Finally, a non linear optimization solver is used to compute the optimal  
78 design, running sequentially the metamodel looking for minima.

79 The remaining part of the paper proceeds as follows: Section 2 examines the  
80 non-intrusive Polynomial Chaos and how it can be used for the robust design  
81 of airships. Next, Section 3 describes how to build the metamodel based on the  
82 kriging theory and which is the best parameterization of the geometry. Then,  
83 the physics, solver and mesh setup of the CFD simulations are described together  
84 with their validation in Section 4. The overall view of the design methodology  
85 is finally given in Section 5, so it can be applied to a realistic case of study in  
86 Section 6. At last, the relevant conclusion are detailed in Section 7.

## 87 **2. Uncertainty Quantification using non-intrusive Polynomial Chaos**

88 As it has been mentioned previously, the NIPC has been selected as the  
89 method of uncertainty quantification. There are other methods than can be  
90 used as alternative, such as Monte Carlo simulations [21] or most probable  
91 point based methods [22]. Many of these methods have proven to have fast  
92 convergence and simple implementation such as those studied by Piazzola *et al.*  
93 [23] and Quagliarella *et al.* [24]. Among those, the NIPC methods have been  
94 used for this work. Alternative methods could be implemented in a similar way.

95 Previous research has established how NIPC can be used to determine the  
96 uncertainty effects in the aerodynamic coefficients [25, 26]. The reader can  
97 refer to [27] and the references therein for the mathematical development of the  
98 theory. Details of how the general theory can be applied to the particular case  
99 of the hull aerodynamics can be found below.

100 In this case, the stochastic function to approximate is the volumetric drag co-  
101 efficient of the hull  $C_{D,v}$ , which is a stochastic function because it depends on (at  
102 least) two stochastic variables: the wind intensity ( $U$ ) and the turbulent levels  
103  $Tu_\infty$ . The NIPC method approximates the stochastic solution  $C_{D,v}(U, Tu_\infty)$   
104 of our design problem by a finite linear combination of orthogonal polynomials

105  $\Phi_i$  of the 2 independent random variable  $\mathbf{S} = (U, Tu_\infty) = (S_1, S_2) \in \mathbb{R}^2$ . So,  
 106 the  $P$ th order approximation can be written as:

$$\mathbf{C}_{\mathbf{D},\mathbf{v}}(\mathbf{S}) \approx \hat{\mathbf{C}}_{\mathbf{D},\mathbf{v}}(\mathbf{S}) := \sum_{i=0}^M \hat{\mathbf{C}}_{\mathbf{D},\mathbf{v},i} \Phi_i(\mathbf{S}), \quad (1)$$

107 where  $\hat{\mathbf{C}}_{\mathbf{D},\mathbf{v},i}$  are the NIPC expansion coefficients, and  $\Phi_i(\mathbf{S})$  are the multivariate  
 108 orthogonal polynomial basis function which can be written in terms of one-  
 109 dimensional polynomial basis function  $\phi_i^{(l_i)}(S_i)$  of each random variable ( $U$  or  
 110  $Tu_\infty$ ) according to the following relation:

$$\Phi_i(\mathbf{S}) = \prod_{i=1}^N \phi_i^{(l_i)}(S_i), \quad (2)$$

111 where  $\sum l_i \leq P$  and the coefficient  $M$  is the total number of basis functions  
 112 and can be calculated as  $M = \binom{N+P}{M}$ .

113 The polynomial base is orthogonal under the following vector product:

$$\langle \phi_i(S_i), \phi_j(S_i) \rangle = \delta_{ij} \langle \phi_i(S_i)^2 \rangle, \quad (3)$$

114 where  $\langle \cdot, \cdot \rangle$  is defined as the expectation operator:

$$\langle f(S_i), g(S_i) \rangle = \int f(S_i)g(S_i)\rho_i(S_i)dS_i, \quad (4)$$

115 being  $\rho_i(S_i)$  the probability density function corresponding to the  $i$ th random  
 116 variable  $S_i$  and  $\delta_{ij}$  the Kronecker delta function.

117 In order to compute each of the coefficients  $\hat{\mathbf{C}}_{\mathbf{D},\mathbf{v},i}$ , we can apply the expecta-  
 118 tion operator to the orthogonal polynomial  $\Phi_i(\mathbf{S})$  which yields to the following  
 119 equation:

$$\hat{\mathbf{C}}_{\mathbf{D},\mathbf{v},i} = \frac{1}{\langle \Phi_i(\mathbf{S})^2 \rangle} \int \mathbf{C}_{\mathbf{D},\mathbf{v}}(\mathbf{S}) \Phi_i(\mathbf{S}) \varrho(\mathbf{S}) d\mathbf{S}. \quad (5)$$

120 where  $\varrho$  is the joint probability density function  $\varrho(\mathbf{S}) = \prod \rho_i(S_i)$ .

121 The integral of Eq. (5) can be approximated by quadrature, so the following  
 122 expression is obtained:

$$\hat{\mathbf{C}}_{\mathbf{D},\mathbf{v},i}(U, Tu_\infty) = \sum_{k_1=1}^{m_1} \sum_{k_2=1}^{m_2} \mathbf{C}_{\mathbf{D},\mathbf{v}}(U_{k_1}, Tu_{\infty k_2}) \frac{\Phi_i(U_{k_1}, Tu_{\infty k_2})}{\langle \Phi_i(U_{k_1}, Tu_{\infty k_2})^2 \rangle} \prod_{j=1}^q \omega_j, \quad (6)$$

123 being  $U_{k_j}$  and  $Tu_{\infty k_j}$  with  $j = 1 \dots q$  the quadrature points of the  $j$ - component  
 124 of the random vector  $\mathbf{S}$ ,  $m_i$  denotes the integration points number of each  
 125 random variable and  $\omega_j$  is the quadrature  $j$ th-dimension weight of the point  
 126  $\mathbf{S}_{k_j}$ .

Once the coefficients have been computed, the expected value  $\mu$  and variance  
 $\sigma$  of  $\mathbf{Y}(\mathbf{S})$  can be estimated using the following equations:

$$\mu(\mathbf{C}_{D,v}) \approx \hat{\mathbf{C}}_{D,v,0}, \quad (7)$$

$$\sigma(\mathbf{C}_{D,v}) \approx \sqrt{\sum_{i=1}^p \langle \phi_i^2 \rangle \hat{\mathbf{C}}_{D,v,i}}. \quad (8)$$

127 Thus, to determine the mean and standard deviation of a particular hull  
 128 design, it is only needed to evaluate that design in each of the quadrature points  
 129 previously defined.

### 130 3. Parameterization and kriging metamodeling

131 Although the NIPC theory reduces the number of CFD simulations needed  
 132 to determine the mean  $C_{D,v}$  of each design, the time that takes to evaluate all  
 133 the quadrature points remains too high. Thus, it is still necessary to create a  
 134 metamodel in order to find the optimal design. That metamodel will compute  
 135 the estimated mean drag coefficient for certain design variables. The number of  
 136 these design variables should be as low as possible although the parameterization  
 137 has to be able to represent the geometry of the hull correctly. That is why  
 138 it is important to correctly choose the shape parameterization. Up to this  
 139 point, there are many families of parameters which can be used to do that.  
 140 For example, Du & Leifur [28] chose B-splines while Mader & Martins [29]  
 141 used Free-form deformation (FFD) instead. However, the CST (Class/Shape  
 142 Transformation) Universal parametric geometry representation method [30] was  
 143 chosen in this case. The main reason is that this method has been shown to  
 144 accurately represent any realistic hull geometry with a minimum number of  
 145 variables [31]. It is worth noting that, in this method, the number of variables



146 to be used can be chosen by the user, depending on the required accuracy. This  
 147 differs from other methods such as the Gertler-58 series, in which the number  
 148 of variables is always 5.

149 A brief description of how to apply it is given below.

150 First, the non-dimensional spatial coordinates are defined as  $\psi = x/c$  and  
 151  $\zeta = y/c$ . Then, the so-called component shape functions are defined as:

$$S_i(\psi) = K_i \psi^i (1 - \psi)^{n-1}, \quad (9)$$

152 in which  $K_i$  is computed with the following formula:

$$K_i = \binom{n}{i} = \frac{n!}{i!(n-i)!}, \quad (10)$$

153 so the overall shape function equation for the upper surface is:

$$Su(\psi) = \sum_{i=1}^n Au_i \cdot S_i(\psi). \quad (11)$$

154 On the other hand, the class function is defined as:

$$C_{N_2}^{N_1}(\psi) = \psi^{N_1} (1 - \psi)^{N_2}, \quad (12)$$

155 and, depending on the the thickness of the trailing edge:

$$\Delta\zeta_{hull} = \frac{y_{TE}}{c}, \quad (13)$$

156 the hull generatrix is given by the following expression:

$$\zeta_{hull} = C_{N_2}^{N_1}(\psi) \cdot Su(\psi) + \psi \cdot \Delta\zeta_{hull}, \quad (14)$$

157 in which the coefficients  $Au_i$  for a particular design can be determined using  
 158 least squares method.

159 Once the geometry parameterization is done, the metamodel creation can be  
 160 started. Kriging techniques interpolate the value of a random field (the mean  
 161  $C_{D,v}$  in our case) at an unknown design parameters from previously compute  
 162 designs. Kriging computes the best linear unbiased estimator (refer from now

163 on as  $\hat{\mathcal{C}}_D(x_0)$ ) based on a stochastic model determined by the expectation and  
164 covariance function of the random field [32].

165 Thus, the kriging metamodel is given by a linear combination [33]:

$$\hat{\mathcal{C}}_D(x_0) = \sum_{i=1}^n w_i(x_0) \mathcal{C}_D(x_i), \quad (15)$$

166 in which the parameters  $w_i$  are computed so the variance:

$$\sigma_k^2(x_0) := \text{Var} \left( \hat{\mathcal{C}}_D(x_0) - \mathcal{C}_D(x_0) \right), \quad (16)$$

167 is minimized subject to the unbiasedness condition:

$$\mathbb{E}[\hat{Z}(x) - Z(x)] = \sum_{i=1}^n w_i(x_0) \mu(x_i) - \mu(x_0) = 0. \quad (17)$$

168 In general, at first, coarse kriging metamodel is generated. Some of the  
169 samples are reserved as test points, so the Mean Square Error  $MSE$  can be  
170 computed as:

$$MSE = \frac{1}{n} \sum_{i=1}^n (\hat{\mathcal{C}}_D(x_i) - \mathcal{C}_D(x_i))^2. \quad (18)$$

171 Then, that error is reduced adding infill points to the model [34, 35].

172 In the present study, the Kriging metamodel has been implemented using  
173 the pyKriging [36] toolbox, recently used in other aerodynamic studies such as  
174 Chen *et al.* [37] and Habermann *et al.* [38].

#### 175 4. CFD model and validations

176 As it has been mentioned before, a large number of CFD simulations are  
177 required to build the stochastic metamodel. To minimize the computational  
178 time, only axysymmetric simulations are considered, which have obtained good  
179 results in previous studies [39] about airship aerodynamics. Steady RANS equa-  
180 tions are solved by the SIMPLE algorithm with a second order upwind scheme  
181 applied to the convection terms. For all the simulations no wall function has  
182 been used and the maximum size of the first cell was selected so  $y^+$  is equal  
183 or less than 1. OpenFoam has been selected as the CFD solver due to: 1) it

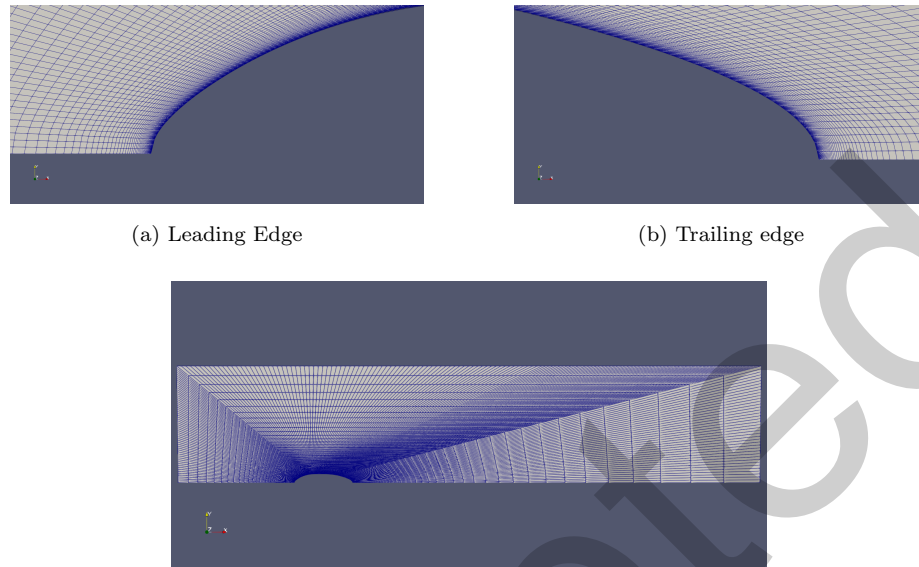


Figure 1: overview of the mesh

184 has been largely proven for external aerodynamics [40], and 2) its automatic  
185 parallelization capabilities. This election is consistent with past studies. For  
186 example, Jouebert and Le Roy [41] studied, using OpenFoam, the effect of the  
187 grid coarseness and numerical schemes on Lighter-than-Air (LTA) aircraft.

188 For each simulation, a rectangular domain and a structured, hexagonal,  
189 2-dimensional mesh around each design was created using the meshing tool  
190 blockMesh, supplied in OpenFoam [42]. Each mesh file has  $2.4 \times 10^4$  cells and  
191 the domain dimensions are  $[-2.5L, 7.5L] \times [-2.5L, 2.5L]$  being the airship (of  
192 length  $L$ ) centered at the point  $(0, 0)$ . An overview of the mesh used can be  
193 seen in Figure 1.

Based on previous work [43][44][5], the RANS model selected is the SST  
Menter  $k - \omega$  [45] although other models such as realizable  $K - \epsilon$  and Spalart-

Allmaras are frequently used [46]. In this model, the equations to solved are:

$$\frac{\partial \bar{u}_i}{\partial x_i} = 0, \quad (19)$$

$$\frac{\partial \bar{u}_i}{\partial t} + \bar{u}_j \frac{\partial \bar{u}_i}{\partial x_j} + u'_j \frac{\partial u'_i}{\partial x_j} = \bar{f}_i - \frac{1}{\rho} \frac{\partial \bar{p}}{\partial x_i} + \nu \frac{\partial^2 \bar{u}_i}{\partial x_j \partial x_j}. \quad (20)$$

The eddy viscosity can be computed as  $\nu_T = \frac{k}{\omega}$ , while  $k$  and  $\omega$  are calculated resolving the following PDEs:

$$\frac{\partial(\rho k)}{\partial t} + \frac{\partial(\rho u_j k)}{\partial x_j} = P - \beta^* \rho \omega k + \frac{\partial}{\partial x_j} \left[ (\mu + \sigma_k \mu_t) \frac{\partial k}{\partial x_j} \right], \quad (21)$$

$$\frac{\partial(\rho \omega)}{\partial t} + \frac{\partial(\rho u_j \omega)}{\partial x_j} = \frac{\gamma}{\nu_t} P - \beta \rho \omega^2 + \frac{\partial}{\partial x_j} \left[ (\mu + \sigma_\omega \mu_t) \frac{\partial \omega}{\partial x_j} \right] + 2(1 - F_1) \frac{\rho \sigma_\omega 2}{\omega} \frac{\partial k}{\partial x_j} \frac{\partial \omega}{\partial x_j}, \quad (22)$$

in which the following closure coefficients and auxiliary relations are used:

$$P = \tau_{ij} \frac{\partial u_i}{\partial x_j}, \quad (23)$$

$$\tau_{ij} = \mu_t \left( 2S_{ij} - \frac{2}{3} \frac{\partial u_k}{\partial x_k} \delta_{ij} \right) - \frac{2}{3} \rho k \delta_{ij}, \quad (24)$$

$$S_{ij} = \frac{1}{2} \left( \frac{\partial u_i}{\partial x_j} + \frac{\partial u_j}{\partial x_i} \right), \quad (25)$$

$$\mu_t = \frac{\rho a_1 k}{\max(a_1 \omega, \Omega F_2)}, \quad (26)$$

$$F_1 = \tanh(\arg_1^4), \quad (27)$$

$$\arg_1 = \min \left[ \max \left( \frac{\sqrt{k}}{\beta^* \omega d}, \frac{500\nu}{d^2 \omega} \right), \frac{4\rho \sigma_\omega 2 k}{CD_{k\omega} d^2} \right], \quad (28)$$

$$CD_{k\omega} = \max \left( 2\rho \sigma_\omega 2 \frac{1}{\omega} \frac{\partial k}{\partial x_j} \frac{\partial \omega}{\partial x_j}, 10^{-20} \right), \quad (29)$$

$$F_2 = \tanh(\arg_2^2), \quad (30)$$

$$\arg_2 = \max \left( 2 \frac{\sqrt{k}}{\beta^* \omega d}, \frac{500\nu}{d^2 \omega} \right). \quad (31)$$

The turbulence free-stream boundary conditions [47] are related to the inflow velocity  $U$  and the turbulent levels  $Tu_\infty$  by the following equations:

$$k = \frac{3}{2} (U Tu_\infty)^2, \quad (32)$$

$$\omega = \frac{\sqrt{k}}{l}, \quad (33)$$

194 in which  $l$  is the turbulent length scale, estimated as the 0.5% of the airship  
 195 length.

196 In order to validate the mesh and CFD configuration, the results obtained  
 197 for the ZHIYUAN-1 [48] are compared with those of Manideep and Rajkumar  
 198 [39] and Wang, Fu, Duan and Shan [48]. The generatrix is given by the following  
 199 equations:

$$y = \begin{cases} f'_r[r_n F_1(z) + k_1 F_2(z) + G_1(z)]^{1/2} & 0 < x < x_m, \quad z = \frac{x}{x_m}, \\ f'_r[s_t^2 F_3(z) + \left(\frac{1-x_m}{x_m}\right)^2 k_1 F_4(z) + G_2(z)]^{1/2} & x_m < x < x_p, \quad z = \frac{1-x}{1-x_m}, \\ f'_r[c_p(1-z)] & x_p < x < 1, \quad z = x, \end{cases} \quad (34)$$

in which:

$$F_1(z) = -2z(z-1)^3, \quad (35)$$

$$F_2(z) = -z^2(z-1)^2, \quad (36)$$

$$G_1(z) = z^2(3z^2 - 8z + 6), \quad (37)$$

$$F_3(z) = -z^2(z-1)^3, \quad (38)$$

$$F_4(z) = -z^3(z-1)^2, \quad (39)$$

$$G_2(z) = z^3(6z^2 - 15z + 10), \quad (40)$$

200 and the constants  $x_m = 0.3935$ ,  $x_p = 0.7570$ ,  $r_n = 0.5071$ ,  $k_1 = 0.2913$ ,  $c_p =$   
 201  $2.7351$ ,  $f'_r = 0.1516$  and  $s_t = 3.2361$ . The CST coefficients will be calculated in  
 202 the Section 6.

203 The case of simulation corresponds to a Reynolds number  $Re = \frac{\rho v L}{\mu} =$   
 204  $2.4 \times 10^6$ .

205 A grid verification study was conducted by varying the number of total cells.  
 206 Five different meshes were tested, the results of which can be seen in Table 1.  
 207 Mesh number 4 was chosen to reduce the calculation time while maintaining  
 208 sufficient accuracy. In all cases, the  $y^+$  number remains below 1.

209 Figure 2 shows a good agreement between studies for the distribution of the  
 210 pressure coefficient  $c_p$ . The  $C_{Dv} = \frac{2D}{\rho V_\infty^2 S}$  obtained is  $2.42 \times 10^{-2}$  which differs  
 211 only a 1.4% from the results of Wang, Fu, Duan & Shan [48] and 5.9% from

Table 1: Grid verification study

Grid	$C_{Dv}$	% difference (finest grid)	N cells
1	$2.19 \times 10^{-2}$	-9.7%	$1.6 \times 10^4$
2	$2.31 \times 10^{-2}$	-5.1%	$1.8 \times 10^4$
3	$2.4 \times 10^{-2}$	-1.2%	$2.0 \times 10^4$
4	$2.42 \times 10^{-2}$	-0.5%	$2.4 \times 10^4$
5	$2.43 \times 10^{-2}$	0	$2.8 \times 10^4$

212 Manideep & Rajkumar [39].

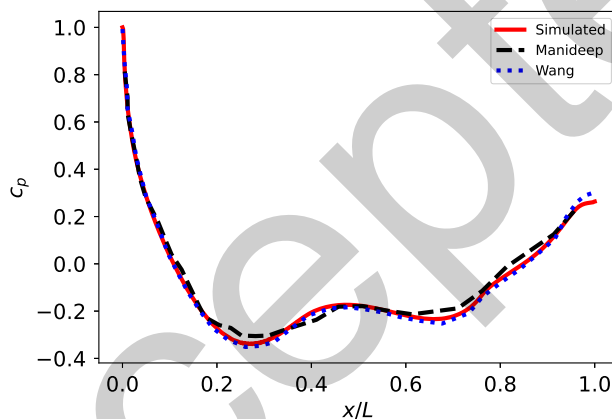


Figure 2: Distribution of  $c_p$  along the airship length.

## 213 5. Design methodology

214 Once the theory of the NIPC and the kriging techniques has been review,  
 215 it is time to join both theories in order to solve the aerodynamic optimization  
 216 problem. That can be resumed into the following steps:

- 217 1. The geometry of a baseline design is parameterized using a certain number  
 218 of parameters. For each of that parameters, its interval of validity is  
 219 determined. The number of variables should be set by the user according  
 220 to the desired accuracy.

- 221 2. The design space, defined by the previous intervals, is randomly sampled,  
222 obtaining  $N$  different hull geometries to evaluate. This is usually done  
223 applying the Latin hypercube sampling technique [49].
- 224 3. Each of the geometries is evaluated, computing its mean  $C_{D,v}$  using the  
225 NIPC.
- 226 4. Once the results are obtained, the first kriging metamodel is created. Some  
227 of the results are used as test points.
- 228 5. To reduce the Mean Squared Error of the model, new infill points are  
229 originated and evaluated.
- 230 6. The previous step is repeated until the MSE is sufficiently small.
- 231 7. Then, the metamodel is ready to be use by any nonlinear programming  
232 solver. The results of the optimization is the geometry which has the lower  
233 mean  $C_{D,v}$ .
- 234 8. Finally, the design can be validated using, for example, a Montecarlo ex-  
235 periment. The results can be also analyzed to gain insights of the problem  
236 physics.

237 In Fig. 3, the flow diagram of the optimization algorithm is shown with all  
238 its relevant parts.

239 It is worth noting that, in this case, the kriging model has as input variables  
240 the geometrical parameters of the hull. The output of the model is the average  
241 drag coefficient, taking into account the probability distribution of the wind  
242 speed and turbulence index. The uncertainty associated with these two variables  
243 should not be confused with that of the kriging model. To train the metamodel,  
244 therefore, a database is required in which we have combinations of geometric  
245 parameters and the average resistance coefficients obtained with them. This  
246 coefficient is estimated for each combination of geometric variables using the  
247 UQ algorithm.

248 Due to the large number of simulations required by the optimization algo-  
249 rithm, an adequate parallelization method should be used. Taking advantage of  
250 the properties of the UQ algorithm, the following method based on supercom-

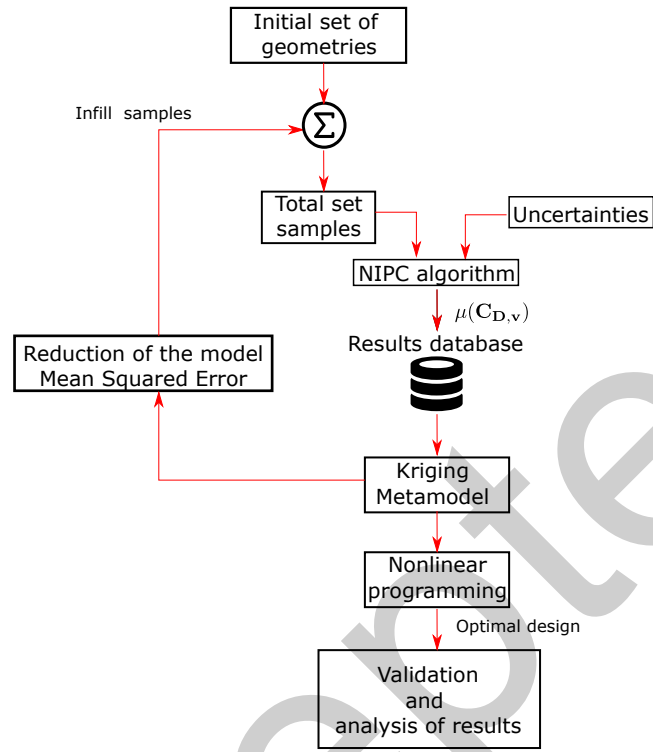


Figure 3: Flow diagram of the proposed optimization algorithm

251 putting is proposed:

- 252 1. For each design, the CFD simulations of all the quadrature points are
- 253 configured in a local workstation.
- 254 2. Then, the different cases are uploaded to the supercomputing center. Each
- 255 of the cases can be run by a different computer node.
- 256 3. Likewise, each of the simulation is easily parallelized inside the node
- 257 thanks to OpenFoam.
- 258 4. Finally, the results are recompile in the local workstation where the meta-
- 259 model is built.

260 Thus, two levels of parallelization can be found. This makes the algorithm  
 261 easily scalable to a higher number of uncertainties, design variables or CFD  
 262 complexity.



263 **6. Case of study**

264 Next, we apply the optimization algorithm to a HAPS airship operating in  
265 the stratosphere (20 km) at a latitude of 30°N. That airship carries 250 kg of  
266 payload which means that its length would be around  $L = 250$  m with today's  
267 technology [1].

268 *6.1. UQ algorithm*

269 Following the statistical study done in previous works [50], the cumulative  
270 distribution of the wind can be computed based on NCEP Reanalysis data  
271 provided by the NOAA/OAR/ESRL PSL, Boulder, Colorado, USA [51]. As it  
272 has been mentioned before, that wind intensity follows a Weibull distribution,  
273 so the probability density function (PDF) is given by the equation:

$$f(t) = \frac{\beta}{\eta} \left( \frac{t - \gamma}{\eta} \right)^{\beta-1} e^{-\left(\frac{t-\gamma}{\eta}\right)^\beta}. \quad (41)$$

in which  $\eta$  is the scale parameter,  $\beta$  is the shape parameter and  $\gamma$  is the location  
parameter. Following a least-squares adjustment, the parameter of the Weibull  
distribution which best fit the observational data are:

$$\eta = 9.715, \quad \beta = 1.672, \quad \gamma = 0.202. \quad (42)$$

274 Hence, the mean wind intensity is 8.9 m/s.

275 Then, it is needed to estimate the probabilistic distributions of the turbu-  
276 lence levels. However, the wind data at that height is scarce and a full study of  
277 the stratospheric characteristics is out of the scope of the present study. In this  
278 study, the approach followed in [26] is adopted: the turbulence levels will be  
279 assumed to follow a normal distribution of mean  $Tu_\infty = 0.07\%$  and standard  
280 deviation  $\sigma = 0.03\%$ .

281 The joint distribution of the wind intensity and turbulence levels affects  
282 the turbulent kinetic energy  $k$  and specific turbulent dissipation rate. Figure 4  
283 shows the different CDFs of the variables which affects the CFD simulations.

284 Once the probabilistic distribution of the wind intensity and turbulence lev-  
285 els is determined, the UQ method has to be configured. Both, the order of

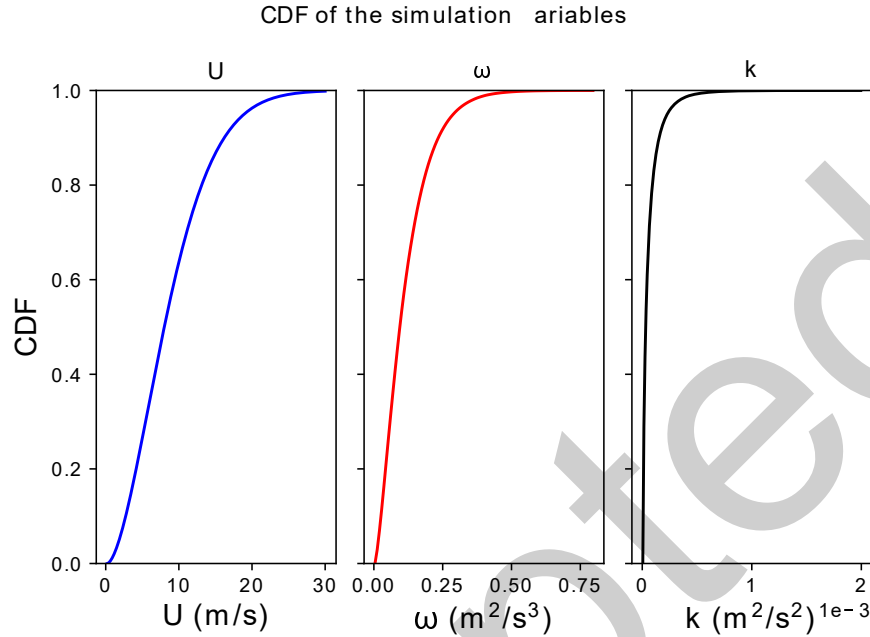


Figure 4: Cumulative distribution function of wind intensity  $U$ , turbulent kinetic energy  $k$  and specific turbulent dissipation rate  $\omega$ .

286 polynomial expansion and the one of quadrature, are set to 3 as a trade-off  
 287 between accuracy and computational cost. Therefore, Equation (5) will be ap-  
 288 proximated by evaluating  $C_{D,v}(U_{k_1}, TL_{k_q})$  at 16 different quadrature points,  
 289 according to Equation (6). In this way, the average resistance coefficient can be  
 290 determined.

## 291 6.2. Metamodel generation

292 After the NIPC model is configured, it is time to build the kriging model.  
 293 The first step is to discretize the hull geometry and determined in which range  
 294 the parameters can varies. As baseline design, the ZHIYUAN-1 geometry was  
 295 selected, given by Equation (34). If the airship length is set to  $L = 250$  m, the  
 296 volume is  $V = 7.5 \times 10^5$  m<sup>3</sup>. The optimization is done for a constant airship  
 297 length (so the Reynolds number is equivalent for all the cases) and volume.

298 Then, the CST method is applied. The number of parameters ( $Au_i$ ) for this  
299 method was fixed to 8 because it was enough to almost replicate the baseline  
300 geometry. These will be the design variables of this case of study. For the  
301 baseline design, this parameter were computed using the least squares methods  
302 obtaining:

$$\begin{aligned} Au_{0b} = 0.0868, \quad Au_{1b} &= 0.1863, \quad Au_{2b} = 0.0354, \quad Au_{3b} &= 0.4371, \\ Au_{4b} = -0.3458, \quad Au_{5b} &= 0.7976, \quad Au_{6b} = -0.2756, \quad Au_{7b} &= 0.7052. \end{aligned}$$

303 In order to find the optimal geometry, we found the metamodel  $\hat{f}$  which com-  
304 pute the mean volumetric drag coefficient in function of that 8 design variables.  
305 To reduce the computational requirements, the design variables are constrained  
306 to the interval  $Au_i \in Au_{ib} \pm 0.05$  although it is enough to represent all the rea-  
307 sonable designs. Firstly, 200 samples were randomly generated by means of the  
308 Latin hypercube sampling technique. These samples are evaluated, each one 14  
309 times (one per quadrature point), and the results are introduced in the kriging  
310 metamodel. From these 200 points, 50 were selected as test points. Then, using  
311 the Mean Square Error  $MSE$  as the infill criteria [52] another 800 samples are  
312 generated and evaluated, of which 200 are test points. Thereafter, the MSE was  
313 small enough ( $MSE < 10^{-3}$ ), so the third phase of the algorithm design can be  
314 started. In any case, the number of kriging points will vary depending on the  
315 required accuracy and the characteristics of the problem in question.

### 316 6.3. Non linear optimization and validation

317 Once the metamodel is finished, it is time to solve the non-linear optimiza-  
318 tion problem. In order to do that, there are different algorithms such as the  
319 Nelder-Mead simplex algorithm or the Sequential Least Squares Programming.  
320 However, the optimal design can be very different from the baseline design, so  
321 it is better to choose a method that could find global minima. Thus, the solver  
322 selected was the differential evolution algorithm described by Storn & Price [53]  
323 and implemented in Scipy [54].

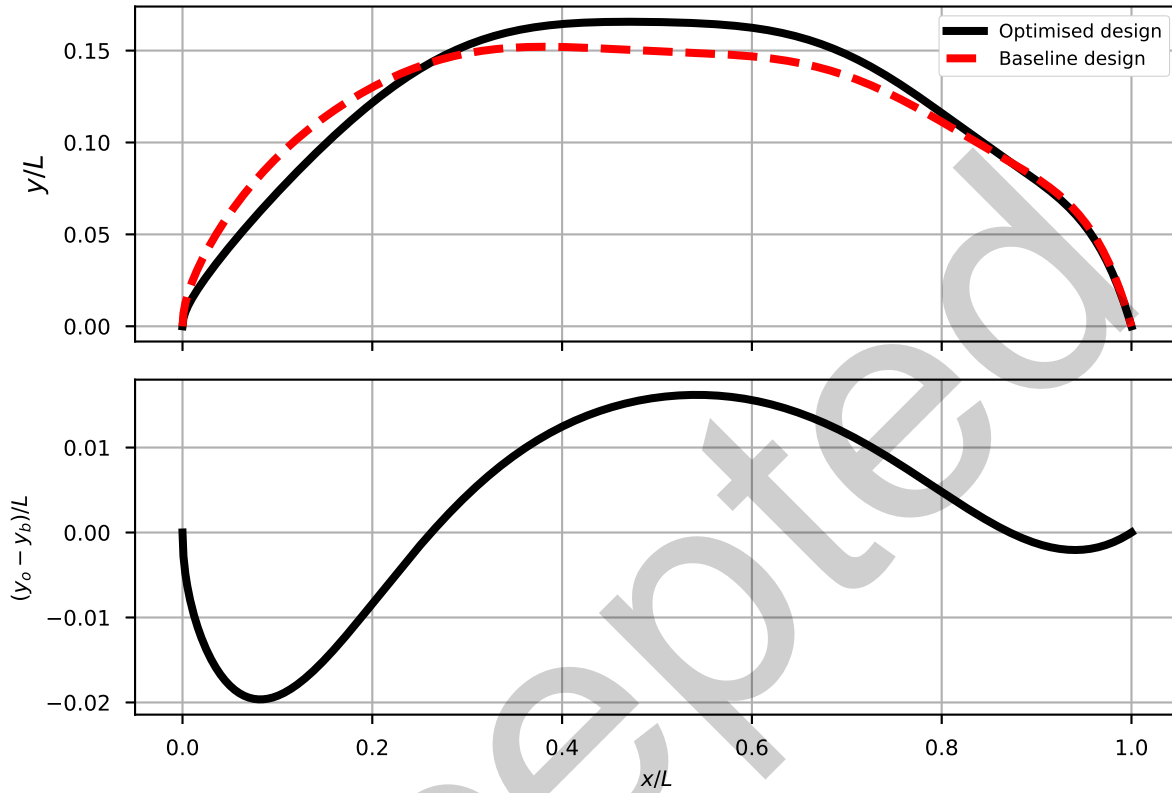


Figure 5: Comparison of the geometries. Top image: optimal hull geometry compared against the baseline design. Bottom image: difference between the optimal design ( $y_o$ ) and the baseline design ( $y_b$ ).

324 The optimal geometry is shown in Figure 5. The thickness ratio (defined  
 325 as the maximum diameter divided by the total length) of the optimal design  
 326 is 8% greater than in the baseline design (0.165 vs 0.152). Furthermore, the  
 327 localization of the maximum thickness moves rearwards: in the optimal design  
 328 it is located at  $x/L = 0.47$  while in the baseline design it is at  $x/L = 0.38$ .

329 Finally, we can verify that the optimal design is actually more robust than  
 330 the baseline design. In order to check that, a Montecarlo experiment is per-  
 331 formed. For both, the baseline and the optimal design,  $10^3$  combinations of  $U$   
 332 and  $Tu_\infty$  are generated and evaluated. The  $C_{D,v}$  distribution for both designs

333 can be found in Figure 6. Indeed, the optimal design achieve a mean  $C_{D,v}$  of  
 334  $2.45 \times 10^{-2}$  instead of the  $2.6 \times 10^{-2}$  achieved by the baseline design, which rep-  
 335 represents an improvement of the 6%. These values can be computed integrating  
 336 the PDF, following the Equation:

$$\mu(C_{D,v}) = \int C_{D,v} \varrho_{C_{D,v}} dC_{D,v} \quad (43)$$

337 where  $\varrho_{C_{V,d}}$  is the PDF of  $C_{V,d}$ . As the hull contribution to the total drag is  
 338 between 60-70%, that is equivalent to a 4% reduction of the total drag. Addi-  
 339 tional improvements can be achieved by optimizing other components such as  
 340 fins or propellers.

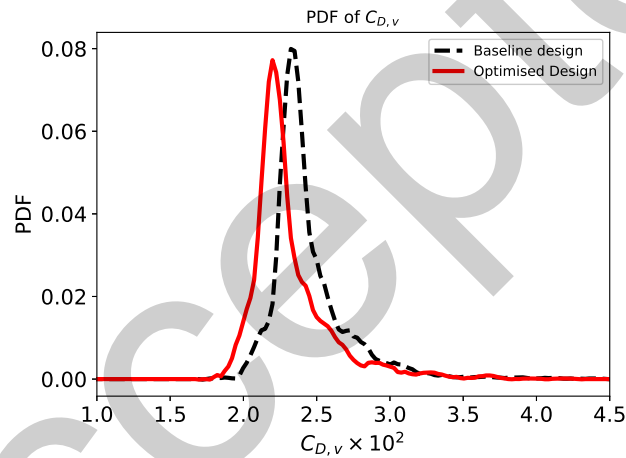


Figure 6: PDF of the  $C_{D,v}$  for both designs.

341 As the optimal design is less flat-nosed than the original one, it is of par-  
 342 ticular interest to analyze how this affects the viscous and pressure forces that  
 343 contributes to the drag. Figure 7 shows the drag coefficient cumulative distribu-  
 344 tion along the airship length. It proofs how the improvement in  $C_{D,v}$  is achieved  
 345 mainly by the reduction of the viscous drag coefficient.

346 Figure 8 shows the velocity field around both airship. The results are in  
 347 accordance with what was shown in Figure 7: optimal design achieves reduced  
 348 overpressure generated at the leading edge in exchange for a slightly increased

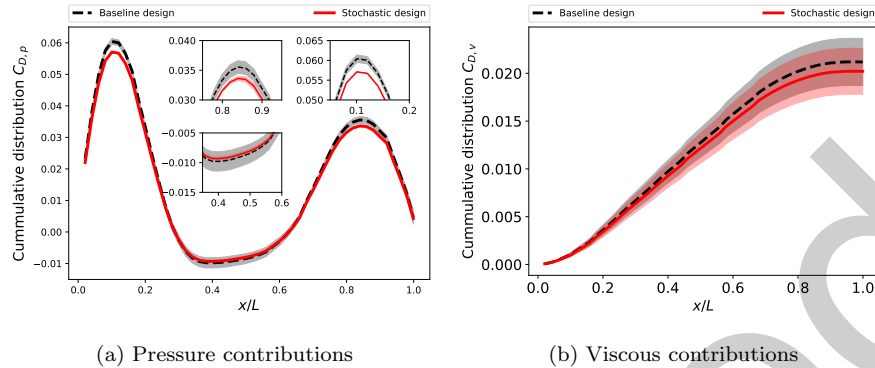


Figure 7: Drag coefficient cumulative distribution along the airship length. The lines are the mean value, and the shading represents the confidence interval.

349 size of the turbulent wake.

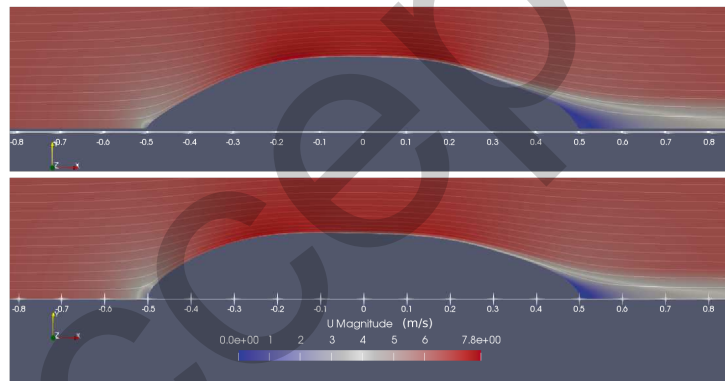


Figure 8: Velocity field for the optimal design (top) and baseline design (bottom).

## 350 7. Conclusions

351 This study has presented a methodology to optimize stratospheric airship  
 352 hulls in an uncertain design scenario. The NIPC theory has been used to com-  
 353 pute the mean volumetric drag coefficient of the proposed hull shapes and two  
 354 sources of uncertainty have been considered: the wind intensity and the tur-  
 355 bulance level at the stratosphere. The NIPC theory can be used to evaluate

356 different design geometries and build a kriging metamodel which, finally, can be  
357 used to found the optimal design.

358 As a particular application, the hull geometry of a HAPS airship has been  
359 optimized. Operating at 20 km and 30°N, we have used as starting point the  
360 geometry of the ZHIYUAN airship for a fixed length of  $L = 250$  m and a volume  
361 of  $7.5 \times 10^5$  m<sup>3</sup>. That volume is enough to carry about 250 kg of payload.  
362 The envelope shape has been discretized using the CST method and the non  
363 linear optimization problem was solved using a genetic algorithm. When the  
364 uncertainties are considered, the shape is more tail-nose.

365 Considering that to evaluate every design under the different flight conditions  
366 it is required to perform several CFD simulations, an adequate parallelization  
367 of the algorithm is desirable, so it can easily escalate for larger cases of study.  
368 In this example, each of the quadrature points is simultaneously evaluated in a  
369 different computing node, obtaining a relevant reduction in the computational  
370 time.

371 In order to check the utility of the present design method, a Montecarlo  
372 experiment has been done generating numerous samples of wind intensity and  
373 turbulence levels. For each sample, the performances of the stochastic and de-  
374 terministic designs have been computed. The results show that the stochastic  
375 design reduces the mission-averaged drag coefficient of the hull by a 6% (ap-  
376 proximately, 4% of the total airship drag). This gain is of utmost importance  
377 for HAPS operations [10, 15].

378 In total, more than 15000 CFD simulations has been done to perform this  
379 study. While that fact might be limiting for many applications, this work is  
380 an example of the new possibilities that the increase in computation power is  
381 bringing.

382 Future work will investigate the hull design under more complex operational  
383 scenarios, including the effect of more variables such as the surface roughness  
384 and how new parallelization schemes can reduce the total computational cost.

385 **Declaration of Competing Interest**

386 The authors declare that there is no conflict of interests regarding the pub-  
387 lication of this article.

388 **Acknowledges**

389 The authors thankfully acknowledge the computer resources at Castilla y  
390 León Supercomputing Center (SCAYLE) and the valuable suggestions of the  
391 anonymous referees that helped to enhance the manuscript.

392 **References**

- 393 [1] J. Gonzalo, D. López, D. Domínguez, A. García, A. Escapa, On the ca-  
394 pabilities and limitations of high altitude pseudo-satellites, *Progress in*  
395 *Aerospace Sciences* 98 (2018) 37–56.
- 396 [2] B. Kirsch, O. Montagnier, Towards the advent of high-altitude pseudo-  
397 satellites (haps), *Disruptive Technology and Defence Innovation Ecosys-*  
398 *tems* 5 (2019) 181–201.
- 399 [3] D. Ma, G. Li, M. Yang, S. Wang, L. Zhang, Shape optimization and ex-  
400 perimental research of near space airship, *Proceedings of the Institution of*  
401 *Mechanical Engineers, Part G: Journal of Aerospace Engineering* 233 (10)  
402 (2019) 3589–3602.
- 403 [4] G. Li, J. Wang, Shape optimization of near-space airships considering the  
404 effect of the propeller, *Journal of Aerospace Engineering* 33 (5) (2020)  
405 04020054.
- 406 [5] X.-Y. Sun, T.-E. Li, G.-C. Lin, Y. Wu, A study on the aero-  
407 dynamic characteristics of a stratospheric airship in its entire  
408 flight envelope, *Proceedings of the Institution of Mechanical*  
409 *Engineers, Part G: Journal of Aerospace Engineering* 232 (5)  
410 (2018) 902–921. arXiv:<https://doi.org/10.1177/0954410017723358>,



- 411 doi:10.1177/0954410017723358.  
412 URL <https://doi.org/10.1177/0954410017723358>
- 413 [6] J. Gonzalo, D. Domínguez, A. García-Gutiérrez, A. Escapa, On  
414 the development of a parametric aerodynamic model of a strato-  
415 spheric airship, *Aerospace Science and Technology* 107 (2020) 106316.  
416 doi:<https://doi.org/10.1016/j.ast.2020.106316>.  
417 URL <https://www.sciencedirect.com/science/article/pii/S1270963820309986>
- 418 [7] X.-Y. Sun, T.-E. Li, G.-C. Lin, Y. Wu, A study on the aerodynamic charac-  
419 teristics of a stratospheric airship in its entire flight envelope, *Proceedings*  
420 *of the Institution of Mechanical Engineers, Part G: Journal of Aerospace*  
421 *Engineering* 232 (5) (2018) 902–921.
- 422 [8] L. Zhang, W. Zhu, H. Du, M. Lv, Multidisciplinary design of high alti-  
423 tude airship based on solar energy optimization, *Aerospace Science and*  
424 *Technology* 110 (2021) 106440.
- 425 [9] L. Zhang, M. Lv, W. Zhu, H. Du, J. Meng, J. Li, Mission-based multidis-  
426 ciplinary optimization of solar-powered hybrid airship, *Energy Conversion*  
427 *and Management* 185 (2019) 44–54.
- 428 [10] M. I. Alam, R. S. Pant, Multi-objective multidisciplinary design analyses  
429 and optimization of high altitude airships, *Aerospace Science and Tech-*  
430 *nology* 78 (2018) 248–259. doi:<https://doi.org/10.1016/j.ast.2018.04.028>.  
431 URL <https://www.sciencedirect.com/science/article/pii/S1270963818302475>
- 432 [11] M. Manikandan, R. S. Pant, Conceptual design optimization of high-  
433 altitude airship having a tri-lobed envelope, in: R. R. Salagame, P. Ramu,  
434 I. Narayanaswamy, D. K. Saxena (Eds.), *Advances in Multidisciplinary*  
435 *Analysis and Optimization*, Springer Singapore, Singapore, 2020, pp. 49–  
436 61.
- 437 [12] J. A. Roney, Statistical wind analysis for near-space applications, *Journal*  
438 *of Atmospheric and Solar-Terrestrial Physics* 69 (13) (2007) 1485–1501.

- 439 [13] M. Lynch, B. Mandadzhiev, A. Wissa, Bioinspired wingtip devices:  
440 a pathway to improve aerodynamic performance during low reynolds  
441 number flight, *Bioinspiration & Biomimetics* 13 (3) (2018) 036003.  
442 doi:10.1088/1748-3190/aaac53.  
443 URL <https://doi.org/10.1088/1748-3190/aaac53>
- 444 [14] D. Kumar, M. Raisee, C. Lacor, *Combination of Polynomial Chaos with*  
445 *Adjoint Formulations for Optimization Under Uncertainties*, Springer In-  
446 *ternational Publishing, Cham, 2019, pp. 567–582. doi:10.1007/978-3-319-*  
447 *77767-2\_35.*  
448 URL [https://doi.org/10.1007/978-3-319-77767-2\\_35](https://doi.org/10.1007/978-3-319-77767-2_35)
- 449 [15] T. D. Economon, F. Palacios, S. R. Copeland, T. W. Lukaczyk, J. J. Alonso,  
450 Su2: An open-source suite for multiphysics simulation and design, *AIAA*  
451 *Journal* 54 (3) (2016) 828–846. arXiv:<https://doi.org/10.2514/1.J053813>,  
452 doi:10.2514/1.J053813.  
453 URL <https://doi.org/10.2514/1.J053813>
- 454 [16] A. G. Liatsikouras, V. G. Asouti, K. C. Giannakoglou, G. Pierrot, M. Mega-  
455 hed, Aerodynamic shape optimization under flow uncertainties using non-  
456 intrusive polynomial chaos and evolutionary algorithms, in: *2nd EC-*  
457 *COMAS Thematic Conference on Uncertainty Quantification in Compu-*  
458 *tational Sciences and Engineering (UNCECOMP 2017)*, Rhodes Island,  
459 Greece, 2017.
- 460 [17] A. Serani, F. Stern, E. F. Campana, M. Diez, Hull-form stochastic op-  
461 timization via computational-cost reduction methods, *Engineering with*  
462 *Computers* (2021) 1–25.
- 463 [18] Z. Liu, M. Yang, J. Cheng, D. Wu, J. Tan, Meta-model based stochastic iso-  
464 geometric analysis of composite plates, *International Journal of Mechanical*  
465 *Sciences* 194 (2021) 106194.
- 466 [19] D. López, D. Domínguez, J. Gonzalo, Impact of turbulence mod-  
467 elling on external supersonic flow field simulations in rocket aerody-

- 468 namics, *International Journal of Computational Fluid Dynamics* 27 (8-  
469 10) (2013) 332–341. arXiv:<https://doi.org/10.1080/10618562.2013.867951>,  
470 doi:10.1080/10618562.2013.867951.  
471 URL <https://doi.org/10.1080/10618562.2013.867951>
- 472 [20] S. Volpi, M. Diez, N. J. Gaul, H. Song, U. Iemma, K. Choi, E. F. Campana,  
473 F. Stern, Development and validation of a dynamic metamodel based on  
474 stochastic radial basis functions and uncertainty quantification, *Structural  
475 and Multidisciplinary Optimization* 51 (2) (2015) 347–368.
- 476 [21] M. Shirzadi, P. A. Mirzaei, M. Naghashzadegan, Improvement of k-epsilon  
477 turbulence model for cfd simulation of atmospheric boundary layer around  
478 a high-rise building using stochastic optimization and monte carlo sampling  
479 technique, *Journal of Wind Engineering and Industrial Aerodynamics* 171  
480 (2017) 366–379.
- 481 [22] X. Du, W. Chen, A most probable point-based method for efficient un-  
482 certainty analysis, *Journal of Design and Manufacturing automation* 4 (1)  
483 (2001) 47–66.
- 484 [23] C. Piazzola, L. Tamellini, R. Pellegrini, R. Broglia, A. Serani, M. Diez,  
485 Comparing multi-index stochastic collocation and multi-fidelity stochastic  
486 radial basis functions for forward uncertainty quantification of ship resis-  
487 tance, arXiv preprint arXiv:2106.00591 (2021).
- 488 [24] D. Quagliarella, A. Serani, M. Diez, M. Pisaroni, P. Leyland, L. Mon-  
489 tagliani, U. Iemma, N. J. Gaul, J. Shin, D. Wunsch, et al., Benchmarking  
490 uncertainty quantification methods using the naca 2412 airfoil with geo-  
491 metrical and operational uncertainties, in: *AIAA Aviation 2019 Forum*,  
492 2019, p. 3555.
- 493 [25] M. Dodson, G. T. Parks, Robust aerodynamic design optimization  
494 using polynomial chaos, *Journal of Aircraft* 46 (2) (2009) 635–646.  
495 arXiv:<https://doi.org/10.2514/1.39419>, doi:10.2514/1.39419.  
496 URL <https://doi.org/10.2514/1.39419>

- 497 [26] A. García-Gutiérrez, J. Gonzalo, D. López, A. Delgado, Stochastic design  
498 of high altitude propellers, *Aerospace Science and Technology* 107 (2020)  
499 106283. doi:<https://doi.org/10.1016/j.ast.2020.106283>.  
500 URL <https://www.sciencedirect.com/science/article/pii/S1270963820309652>
- 501 [27] S. Hijazi, G. Stabile, A. Mola, G. Rozza, Non-intrusive polynomial chaos  
502 method applied to full-order and reduced problems in computational fluid  
503 dynamics: a comparison and perspectives, in: *Quantification of Uncer-*  
504 *tainty: Improving Efficiency and Technology*, Springer, 2020, pp. 217–240.
- 505 [28] X. Du, L. Leifsson, Optimum aerodynamic shape design under uncertainty  
506 by utility theory and metamodeling, *Aerospace Science and Technology* 95  
507 (2019) 105464.
- 508 [29] C. A. Mader, J. R. R. A. Martins, Stability-constrained aerodynamic shape  
509 optimization of flying wings, *Journal of Aircraft* 50 (5) (2013) 1431–1449.  
510 arXiv:<https://doi.org/10.2514/1.C031956>, doi:10.2514/1.C031956.  
511 URL <https://doi.org/10.2514/1.C031956>
- 512 [30] B. Kulfan, J. Bussoletti, "fundamental" parametric geometry representa-  
513 tions for aircraft component shapes, 2006, pp. 1–10. doi:10.2514/6.2006-  
514 6948.
- 515 [31] B. Kulfan, Recent Extensions and Applications of the "CST"  
516 Universal Parametric Geometry Representation Method, Ch. 5,  
517 pp. 1–10. arXiv:<https://arc.aiaa.org/doi/pdf/10.2514/6.2007-7709>,  
518 doi:10.2514/6.2007-7709.  
519 URL <https://arc.aiaa.org/doi/abs/10.2514/6.2007-7709>
- 520 [32] D. R. Jones, A taxonomy of global optimization methods based on response  
521 surfaces, *Journal of global optimization* 21 (4) (2001) 345–383.
- 522 [33] A. Forrester, A. Sobester, A. Keane, *Engineering design via surrogate mod-*  
523 *elling: a practical guide*, John Wiley & Sons, 2008.

- 524 [34] L. Yaohui, A kriging-based global optimization method using multi-points  
525 infill search criterion, *Journal of Algorithms & Computational Technology*  
526 11 (2017) 174830181772530. doi:10.1177/1748301817725307.
- 527 [35] J. Liu, Z.-H. Han, W. Song, Comparison of infill sampling criteria in  
528 kriging-based aerodynamic optimization, 28th Congress of the International  
529 Council of the Aeronautical Sciences 2012, ICAS 2012 2 (2012) 1625–1634.
- 530 [36] C. Paulson, G. Ragkousis, pykriging: A python kriging toolkit (Jul. 2015).  
531 doi:10.5281/zenodo.21389.  
532 URL <https://doi.org/10.5281/zenodo.21389>
- 533 [37] H. Chen, L. He, W. Qian, S. Wang, Multiple aerodynamic coefficient pre-  
534 diction of airfoils using a convolutional neural network, *Symmetry* 12 (4)  
535 (2020). doi:10.3390/sym12040544.  
536 URL <https://www.mdpi.com/2073-8994/12/4/544>
- 537 [38] A. L. Habermann, R. Zahn, A. Seitz, M. Hornung, Multidimen-  
538 sional Parametric Study of a Propulsive Fuselage Concept Using  
539 OpenFOAM. arXiv:<https://arc.aiaa.org/doi/pdf/10.2514/6.2020-2754>,  
540 doi:10.2514/6.2020-2754.  
541 URL <https://arc.aiaa.org/doi/abs/10.2514/6.2020-2754>
- 542 [39] M. D. Reddy, R. S. Pant, CFD analysis of axisymmetric bodies of revolution  
543 using OpenFOAM. arXiv:<https://arc.aiaa.org/doi/pdf/10.2514/6.2018-3334>,  
544 doi:10.2514/6.2018-3334.  
545 URL <https://arc.aiaa.org/doi/abs/10.2514/6.2018-3334>
- 546 [40] C. Suvanjumrat, Comparison of turbulence models for flow past naca0015  
547 airfoil using openfoam, *Engineering Journal* 21 (3) (2017) 207–221.
- 548 [41] G. Joubert, J.-F. Roy, Open-source cfd code assesement for lighter-than-  
549 air aerodynamic flows simulations, 2017.

- 550 [42] G. Chen, Q. Xiong, P. J. Morris, E. G. Paterson, A. Sergeev, Y. Wang,  
551 Openfoam for computational fluid dynamics, *Notices of the AMS* 61 (4)  
552 (2014) 354–363.
- 553 [43] G. Carbone, G. Martinat, D. Farcy, J.-L. Harion, Aerodynamic investi-  
554 gation of a 3.5: 1 prolate spheroid, in: *AIAA AVIATION 2020 FORUM*,  
555 2020, p. 3053.
- 556 [44] Cui Yanxiang, Yang Yanchu, Zhou Jianghua, Zhang Xiangqiang, Yan feng,  
557 Numerical aerodynamic investigations on stratospheric airships of different  
558 tail configurations, in: *2015 IEEE Aerospace Conference*, 2015, pp. 1–9.  
559 doi:10.1109/AERO.2015.7118977.
- 560 [45] F. R. Menter, Improved two-equation k-omega turbulence models for aero-  
561 dynamic flows, *Nasa Sti/recon Technical Report N 93 (1992) 22809*.
- 562 [46] Y. K. Chen, X. Zhang, Cfd-rans model validation of turbulent flow:  
563 A case study on maat airship, in: *Proceedings of 2014 International*  
564 *Conference on Modelling, Identification Control*, 2014, pp. 254–258.  
565 doi:10.1109/ICMIC.2014.7020761.
- 566 [47] F. R. Menter, Two-equation eddy-viscosity turbulence models for engineer-  
567 ing applications, *AIAA journal* 32 (8) (1994) 1598–1605.
- 568 [48] X.-L. Wang, G.-Y. Fu, D.-P. Duan, X.-X. Shan, Experimental investiga-  
569 tions on aerodynamic characteristics of the zhiyuan-1 airship, *Journal of*  
570 *aircraft* 47 (4) (2010) 1463–1468.
- 571 [49] R. L. Iman, *Latin hypercube sampling*, *Wiley StatsRef: Statistics Refer-*  
572 *ence Online* (2014).
- 573 [50] A. García-Gutiérrez, J. Gonzalo, D. Domínguez, D. López, A. Es-  
574 capa, Aerodynamic optimization of propellers for high altitude  
575 pseudo-satellites, *Aerospace Science and Technology* 96 (2020) 105562.  
576 doi:<https://doi.org/10.1016/j.ast.2019.105562>.  
577 URL <https://www.sciencedirect.com/science/article/pii/S1270963819323375>

- 578 [51] E. Kalnay, M. Kanamitsu, R. Kistler, W. Collins, D. Deaven, L. Gandin,  
579 M. Iredell, S. Saha, G. White, J. Woollen, et al., The ncep/ncar 40-year  
580 reanalysis project, *Bulletin of the American meteorological Society* 77 (3)  
581 (1996) 437–472.
- 582 [52] J. Sacks, W. J. Welch, T. J. Mitchell, H. P. Wynn, Design and analysis of  
583 computer experiments, *Statistical science* (1989) 409–423.
- 584 [53] R. Storn, K. Price, Differential evolution—a simple and efficient heuristic for  
585 global optimization over continuous spaces, *Journal of global optimization*  
586 11 (4) (1997) 341–359.
- 587 [54] P. Virtanen, R. Gommers, E. Burovski, T. E. Oliphant, D. Cournapeau,  
588 W. Weckesser, P. Peterson, N. Mayorov, S. van der Walt, J. Wilson, et al.,  
589 *scipy/scipy: Scipy 1.2. 1*, Zenodo (2019).

[Click here to access/download](#)

**Source File [LaTeX/Word.doc]**  
stochasticOptimization\_v1.5.tex

ACCEPTED



# Declaration of Competing Interest

The authors declare that there is no conflict of interests regarding the publication of this article.

Accepted